Tricritical Ising Edge Modes in a Majorana-Ising Ladder

by

Chengshu Li

B.Sc., Tsinghua University, 2015

A THESIS SUBMITTED IN PARTIAL FULFILLMENT OF
THE REQUIREMENTS FOR THE DEGREE OF

MASTER OF SCIENCE

in

The Faculty of Graduate and Postdoctoral Studies

(Physics)

THE UNIVERSITY OF BRITISH COLUMBIA

(Vancouver)

July 2017

Abstract

While Majorana fermions remain at large as fundamental particles, they emerge in condensed matter systems with peculiar properties. Grover *et al.* [1] proposed a Majorana-Ising chain model, or the GSV model, where the system undergoes a tricritical Ising transition by tuning just one parameter. In this work, we generalize this model to a ladder with inter-chain Majorana couplings. From a mean field analysis, we argue that the tricritical Ising transition will also occur with inter-chain couplings that allow the system to be gapless in the non-interacting case. More crucially, based on analysis of the interacting chain model and the non-interacting ladder model, we expect the tricritical Ising modes to appear on the edges, a feature that might persist when going to 2d. We carry out extensive DMRG calculations to verify the theory in the ladder model. Finally, we discuss possible numerical probes of a 2d model.

Lay Summary

In solid state systems, particles that do not exist in vacuum can emerge, with interesting properties and possible applications to new materials and devices. Furthermore, one can assembly these particles in a sophisticated way that allows even more bizarre behaviors. In this work we propose such a model, which has a configuration of a ladder, and its properties are studied both analytically and numerically.

Preface

This thesis is original, unpublished, independent work by the author, Chengshu Li.

Table of Contents

Appendix

List of Tables

List of Figures

Acknowledgements

First of all, I would like to extend my thanks to my supervisor, Prof. Marcel Franz, who has patiently helped me throughout my research. I have been deeply impressed and influenced by his taste and insights in physics. I would like to thank Dr. Miles Stoudenmire for developing the DMRG library ITensor. I would like to thank Dr. Miles Stoudenmire and Prof. Lukasz Cincio for providing timely advice on various technical details. I would also like to thank Dr. Dmitry Pikulin, Dr. Armin Rahmani, Xiaoyu Zhu, Étienne Lantagne-Hurtubise, Oğuzhan Can, Tianyu Liu, Anffany Chen, Enrique Colomés and Dr. Emilian Nica for helpful discussions. Finally, I would like to thank my family for their support.

Chapter 1

Introduction

In this chapter we discuss the background and main concerns of the thesis. We first introduce the Majorana-Ising chain model, or the GSV model, which motivates our work. A more technical discussion is detailed in Chapter 2. Then we discuss the features of the model that motivates a generalization to a ladder/2d model. We also briefly discuss possible experimental realizations of the models.

1.1 The GSV model

Grover, Sheng and Vishwanath[1] came up with a Majorana-Ising chain model in 2014. For a background discussion on Majorana fermions, see Appendix A. We postpone the detailed analysis of the model till Chapter 2 and only sketch the physics in this section. The model is shown in Fig. 1.1. The nearest neighbor couplings between the Majorana fermions are modulated by an Ising spin field, which in turn has nearest neighbor longitudinal antiferromagnetic Ising couplings and experiences a transverse magnetic field h.

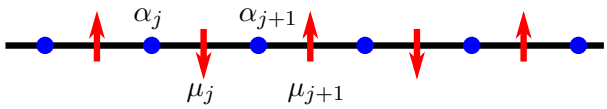

Figure 1.1: Majorana-Ising chain model, or the GSV model.

In this model, if one fixes all other parameters and tunes h, there will be three different phases. For small h, the system is gapped, while for large h the system is gapless and in a critical Ising phase. For a particular value of h, a tricritical Ising (TCI) transition will occur. The phase diagram is shown in Fig. 1.2.

Compared with other known models, this is the first model where a TCI is obtained by tuning only one parameter. Moreover, it is known that the

TCI is supersymmetric in an algebraic sense[2], which means that supersymmetry, a long-expected but elusive ingredient of various grand unified theories, is realized in a condensed matter system.

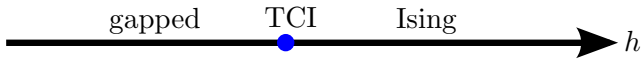

Figure 1.2: The phase diagram of the GSV model.

1.2 The TCI edge mode and the ladder/2d model

Now we focus on the TCI point. From the low energy field theoretic point of view, there is a left-moving mode and a right-moving mode. A natural question is, can we separate the left- and right- movers into different edges? Behaviour of this kind is familiar in various quantum Hall effects and give rise to interesting phenomena, e.g. the quantized conductance. A separation of left- and right- movers will keep them from being gapped out by local couplings, and will in turn stabilize the edge modes. Thus we expect a stable TCI phase when we go to 2d.

As a first step to constructing a 2d model, we consider coupling two chains to form a ladder model. We resort to the non-interacting model for a coupling scheme, see Section 3.2 for a thorough discussion. It is known that if one introduces a direct coupling t_1 and a diagonal coupling t_2 between two chains, as in Fig. 3.2, we will have edge modes when $t_1 = 2t_2$. We introduce this coupling scheme to the Majorana-Ising model, and expect that a TCI edge mode will emerge with appropriate parameters. In this work we show that this indeed is the case by both analytical and numerical argument.

A logical generalization is then a 2d model. However, the numerical technique used in the chain and ladder model, the density matrix renormalization group (DMRG), is not applicable in 2d. In the last part of this thesis, we discuss a possible numerical approach and apply it to the non-interacting system.

1.3 Possible experimental realizations

In the original GSV model, Grover *et al.* proposed a potential realization at the surface of a slab of He_3-B, where Majorana modes are expected to

emerge. The phase transition is driven by a magnetic field parallel to the surface. We expect that our model can also be realized in this setup.

Chapter 2

The GSV model

In this chapter we discuss the model and relevant technical background. We first give a detailed discussion of the GSV model in Section 2.1. Then we introduce in Section 2.2 the conformal field theory, a powerful and versatile tool that we rely on heavily throughout the work. We briefly review the numerical technique, DMRG, in Section 2.3. Finally, we present the numerical results of the GSV model in Section 2.4.

2.1 A detailed discussion of the model

The Hamiltonian of the GSV model is

$$\begin{aligned} H &= H_{\mathrm{M}} + H_{\mathrm{Ising}} + H_{\mathrm{g}} \\ H_{\mathrm{M}} &= it \sum_j \alpha_j \alpha_{j+1} \\ H_{\mathrm{Ising}} &= J \sum_j \mu_j^z \mu_{j+1}^z - h \sum_j \mu_j^x \\ H_{\mathrm{g}} &= -igt \sum_j \alpha_j \alpha_{j+1} \mu_j^z \end{aligned} \tag{2.1}$$

We examine each term in detail. H_{M} is a tight binding model for Majorana fermions, where the i guarantees hermiticity. For reasons that will become clear shortly, we consider a slightly more general Hamiltonian

$$H'_{\mathrm{M}} = it_1 \sum_j \alpha_j \beta_j + it_2 \sum_j \beta_j \alpha_{j+1} \tag{2.2}$$

where $t_1, t_2 > 0$, and $H'_{\mathrm{M}} = H_{\mathrm{M}}$ when $t_1 = t_2 = t$. The bulk spectrum is readily obtained by going to momentum space

$$\begin{aligned}
\alpha_k &= \sqrt{\frac{1}{2N}} \sum_j e^{ikj} \alpha_j \\
\alpha_j &= \sqrt{\frac{2}{N}} \sum_k e^{-ikj} \alpha_k \\
\beta_k &= \sqrt{\frac{1}{2N}} \sum_j e^{ikj} \beta_j \\
\beta_j &= \sqrt{\frac{2}{N}} \sum_k e^{-ikj} \beta_k
\end{aligned} \tag{2.3}$$

where N is the size for α and β (thus the total size is $2N$). We have set the lattice constant to be 1 for simplicity and chosen a normalization so that

$$\{\alpha_k^\dagger, \alpha_{k'}\} = \{\beta_k^\dagger, \beta_{k'}\} = \delta_{kk'} \tag{2.4}$$

In momentum space the Hamiltonian is

$$H'_{\mathrm{M}} = \sum_k i(t_1 - e^{ik} t_2) \alpha_k^\dagger \beta_k - i(t_1 - e^{-ik} t_2) \beta_k^\dagger \alpha_k \tag{2.5}$$

We obtain the spectrum upon diagonalization

$$E = \sqrt{t_1^2 + t_2^2 - 2t_1 t_2 \cos k} = \sqrt{(t_1 - t_2)^2 + 4t_1 t_2 \sin^2 \frac{k}{2}} \tag{2.6}$$

The spectrum is gapped when $t_1 \neq t_2$, and becomes gapless at $t_1 = t_2$. Interestingly, the gaplessness is related to the phase transition of the transverse field Ising model. To see that we perform a Jordan-Wigner transformation

$$\begin{aligned}
\alpha_j &= \sigma_j^x \prod_{k<j} \sigma_k^z \\
\beta_j &= \sigma_j^y \prod_{k<j} \sigma_k^z
\end{aligned} \tag{2.7}$$

and the Hamiltonian now reads

$$H'_{\mathrm{M}} = -t_1 \sum_j \sigma_j^z - t_2 \sum_j \sigma_j^x \sigma_{j+1}^x \tag{2.8}$$

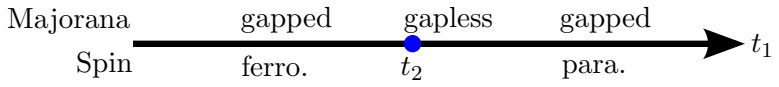

Figure 2.1: Phase diagram of the t_1-t_2 model. In the Majorana representation (up), $t_1 = t_2$ is the gapless point. In the spin representation (down), $t_1 < t_2$ and $t_1 > t_2$ corresponds to ferromagnetic and paramagnetic phases, respectively.

We can interpret t_1 as the transverse magnetic field and t_2 as the ferromagnetic Ising coupling. Now the two phases of $t_1 > t_2$ and $t_1 < t_2$ correspond to the paramagnetic and the ferromagnetic phase, respectively, and the phase transition is equivalent to an Ising one.

H_{Ising} is a transverse field antiferromagnetic Ising model. We can map it into the familiar ferromagnetic one by rotating the spins on the even sites by π around the x-axis

$$\begin{aligned} U &= \prod_{\text{even } j} \exp\left(i\frac{\pi}{2}\mu_j^x\right) \\ U^{-1}H_{\text{Ising}}U &= -J\sum_j \mu_j^z\mu_{j+1}^z - h\sum_j \mu_j^x \end{aligned} \tag{2.9}$$

Thus the phase transition occurs at $J = h$.

Finally, H_{g} couples the spin and Majorana degrees of freedom. This term breaks the $\mathbb{Z}_2$ symmetry of H_{Ising}.

The interaction term H_{g} thwarts an exact solution, and as a first step toward understanding we resort to a mean field theory (MFT) analysis. Fortunately, much of the physics is already captured from this very simple approach.

The assumption we make is that the spin degree of freedom in H_{g}, μ^z, is not dynamical, but enters only as a parameter, which is in turn determined by H_{Ising}. In other word, we make the MFT substitution

$$H_{\text{g}} = -igt\sum_j \alpha_j\alpha_{j+1}\mu_j^z \to H_{\text{MFT}} = -igt\sum_j \alpha_j\alpha_{j+1}\langle\mu_j^z\rangle \tag{2.10}$$

Now we go to the two limiting cases of $h \to \infty$ and $h \to 0$. When $h \to \infty$, all the spins align in the x-direction, leaving $\langle\mu_j^z\rangle = 0$. Thus the interacting term vanishes, and H_{M} is in a gapless phase of the Ising class.

When $h \to 0$, the spins are antiferromagnetically ordered, with $\langle\mu_j^z\rangle = (-1)^j$. Then $H_{\text{M}} + H_{\text{MFT}}$ is equivalent to the t_1-t_2 model discussed in the previous section, and the spectrum is gapped.

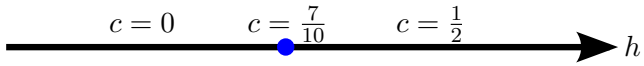

Figure 2.2: Phase diagram from MFT analysis. To make contact with the numerical results in Section 2.4, we have label the three phases with the central charge c, also see Table 2.1.

When tuning h from 0 to ∞, the system evolves from a gapped phase to an Ising phase, thus we expect a TCI phase transition in between. Numerical results are shown in Section 2.4.

2.2 Conformal field theory in $1+1$D

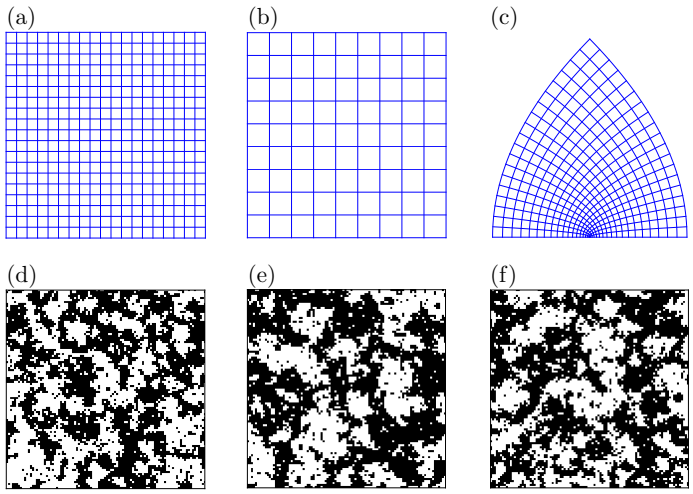

Figure 2.3: Conformal invariance and phase transitions. (a)(b) and (a)(c) show two conformal transformations $z \to w_1 = 2z$ and $z \to w_2 = z^2$. (d)(e)(f) Under these transformations the configuration of a critical Ising model is "invariant", the definite meaning of which is clarified in CFT.

At second-order phase transitions, the correlation length diverges, and an emergent scaling invariance is realized. In the critical regime, one can further assume conformal invariance, an even larger symmetry to be defined

shortly[3][2][4]. Conformal field theory (CFT) is developed to fully exploit the conformal invariance in the formulation of field theory. In $1+1$D or $2+0$D in particular, conformal invariance is so restrictive that quite a lot of results can be deduced based on only a few assumptions. We utilize only $1+1$D CFT in this work.

Conformal transformation is defined by

$$g_{\mu\nu}(x) \to g'_{\mu\nu}(x') = \Omega(x) g_{\mu\nu}(x) \tag{2.11}$$

where $g_{\mu\nu}(x)$ is the metric tensor and $\Omega(x)$ is a scalar field. In $1+1$D, this corresponds to all analytic coordinate transformations $z \to f(z)$, where we have gone to complex coordinates $z = x+iy$ and we measure space and time coordinates in the same unit by setting $v = 1$. A system can be described by CFT if there exist fields called primary fields which transform according to

$$\Phi(z,\bar{z}) \to \left(\frac{\partial f}{\partial z}\right)^{h} \left(\frac{\partial \bar{f}}{\partial \bar{z}}\right)^{\bar{h}} \Phi\left(f(z), \bar{f}(\bar{z})\right) \tag{2.12}$$

where h and $\bar{h}$ are real numbers known as conformal weights.

An important parameter in CFT is the central charge c, defined through the radially ordered operator product expansion (OPE)

$$R\left(T(z)T(w)\right) = \frac{c/2}{(z-w)^4} + \frac{2}{(z-w)^2} T(w) + \frac{1}{z-w} \partial T(w) \tag{2.13}$$

Here, $T(z)$ is the stress-energy tensor, and R denotes radial ordering. Imposing a unitary condition on the theory, one can show that only a few discrete values of c are allowed, each can be identified with some phase transition classes. Thus, c provides an easy probe for the identification of a phase transition. In this work we focus on the tricritical Ising transition (TCI), with central charge $c = \frac{7}{10}$.

2.3 DMRG algorithm

Interacting systems are notoriously hard to solve numerically, mainly due to the fact that the dimension of the Hilbert space grows exponentially with the system size. As a classical example, the Hilbert space of the Hubbard model is 4^N and is as large as $4^{800} \simeq 10^{480}$ for a moderate system size of $20 \times 20 \times 20$. As a result, only systems of relatively small sizes can be solved by brute force.

Fortunately, for (quasi-)1D system, a good ansatz known as the matrix product state (MPS)[5] turns out to give an almost accurate ground state

wavefunction. The basic idea is to rewrite the wavefunction in terms of products of matrices by singular value decomposition (SVD)

$$\psi_{i_1,i_2,\cdots,i_n} = \sum_{j_1,j_2,\cdots,j_{n-1}} A^{j_1}_{i_1} A^{j_1,j_2}_{i_2} \cdots A^{j_{n-2},j_{n-1}}_{i_{n-1}} A^{j_{n-1}}_{i_n} \tag{2.14}$$

Within each step, we truncate the matrix by keeping only the dominant singular values. From the modern view, the density matrix renormalization group (DMRG) is a variational method based on MPS. The computational cost is only $\mathcal{O}(Lm^3)$, where L is the system size and m is the bond dimension of MPS, typically $10^2 \sim 10^3$. The efficiency comes from the fact that in 1D the entanglement between two subsystems grows only logarithmically, a special case of the area law. In this work we carry out extensive DMRG calculations to obtain the ground state with a cutoff error as small as 10^{-6}.

2.4 DMRG results

We apply finite DMRG algorithm to calculate the ground state wavefunction of the full Hamiltonian with periodic boundary condition using ITensor[6]. We have again performed Jordan-Wigner transformation so that the Hamiltonian is spin-$\frac{1}{2}$ only, which is easier for numerical simulations. The Hamiltonian is

$$\begin{aligned} H = &-t\sum_j(\sigma^x_j\sigma^x_{j+1} - \sigma^z_j) + gt\sum_j(\sigma^x_j\sigma^x_{j+1}\mu^z_{j,a} - \sigma^z_j\mu^z_{j,b}) \\ &+ J\sum_j(\mu^z_{j,a}\mu^z_{j,b} + \mu^z_{j,b}\mu^z_{j+1,a}) - h\sum_j(\mu^x_{j,a} + \mu^x_{j,b}) \end{aligned} \tag{2.15}$$

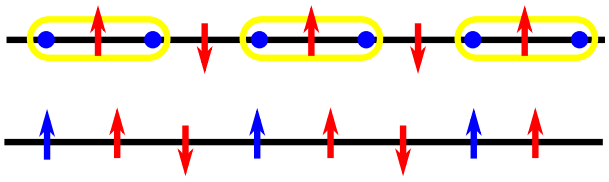

Figure 2.4: The pure spin model after Jordan-Wigner transformation.

As discussed in Section 2.2, the main weapon at our disposal is the central charge c. The central charges of some common CFTs are shown in Table 2.1. In order to extract the central charge, we measure the entanglement entropy

CFT	central charge c
vacuum	0
free fermions/Ising	$\frac{1}{2}$
free bosons	1
tricritical Ising	$\frac{7}{10}$

Table 2.1: A dictionary for the central charges of some common CFTs.

S_A of subsystems of various sizes from the ground state wavefunction. S_A is defined from the reduced density matrix ρ_A

$$S_A = \mathrm{Tr}(\rho_A \ln \rho_A) \tag{2.16}$$

where $\rho_A = \mathrm{Tr}_B \rho$. S_A is related to central charge c by the famous formula[7]

$$S_A = \frac{c}{3} \ln \left[\frac{L}{\pi a} \sin \left(\frac{\pi l_A a}{L} \right) \right] + S_0 \tag{2.17}$$

where l_A and L are lengths of the subsystem and the whole system, respectively, a is the lattice constant, and S_0 is a constant independent of l_A. A typical fitting is shown in Fig. 2.5.

Our main results are shown in Fig. 2.6, in agreement with Grover *et al.*'s results.

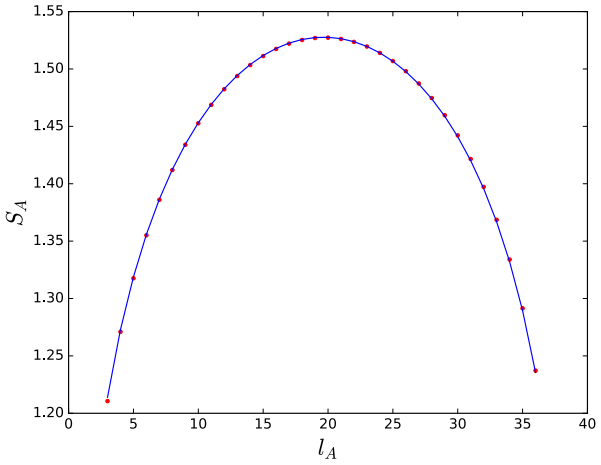

Figure 2.5: A typical fitting of the central charge with Eq. 2.17. We omit the points $l_A \sim 1$ because the CFT prediction works at long distances.

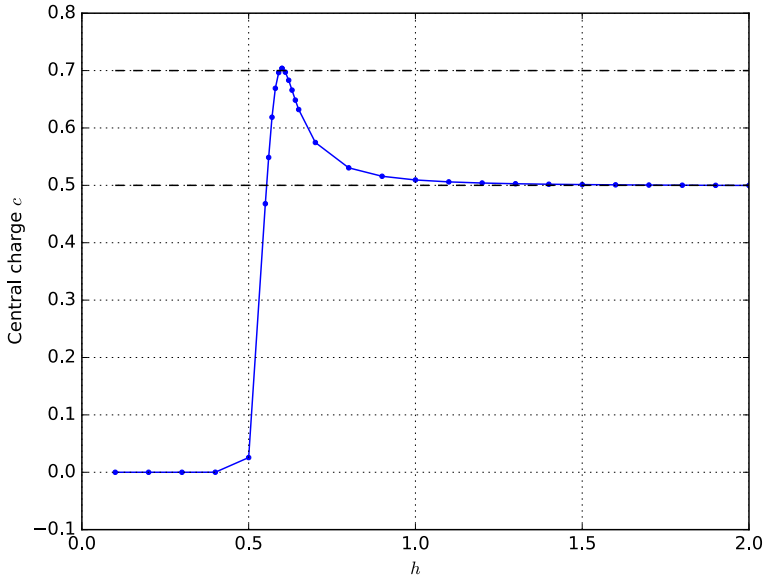

Figure 2.6: DMRG result of the Majorana-Ising chain model. Here we have $L = 80,\ g = 1,\ J = 0.3$.

Chapter 3

Majorana-Ising ladder

In this chapter the main results of this research project are presented. We provide some general remarks in Section 3.1, motivating the generalization to a ladder and eventually to 2d. Then in Section 3.2 we discuss the non-interacting Majorana ladder model, which, while serving as the MFT approximation of the fully interacting model, is of great interest on its own. The fully interacting model is introduced and analyzed in Section 3.3, where we argue the existence of the TCI chiral edge modes, the key result of this work. Finally, the numerics we perform to support the analytical argument are summarized in Section 3.4.

3.1 General remarks

Based on the discussions so far, we want to generalize the model to 2d, where richer physics is expected. We briefly discuss two aspects therein.

Edge physics and edge-bulk correspondence. The edge-bulk correspondence is an echoing feature in topological phases. It appears already in 1d systems such as the Su-Schrieffer-Heeger model[8], where the edge charge is determined by the bulk phase. In 2d an archetypal example is the quantum Hall effect (QHE), one of the first and most thoroughly studied topological phases. In QHE the experimentally observed quantized conductance boils down to the chiral edge modes, or equivalently a topological invariance of the bulk states, a surprising connection bridged by Thouless, Kohmoto, Nightingale and Den Nijs[9]. While in QHE the bulk is exactly solvable, in the current situation the edge is more easily probed thanks to CFT. We thus expect an investigation of the edge physics interesting and informative.

Anyons in 2d. In 1d, particles can not pass through each other, and there is no difference between bosons and fermions. In $d \geq 3$, there is only one topologically (more precisely, homotopically) equivalent way of exchanging

two identical particles, and thus the unitary transformation of exchanging N particles is given by the representation of the permutation group S_N. Indeed, bosons correspond to the trivial representation and fermions correspond to another 1-d representation. In 2d, however, when particles exchange the worldlines can braid in an infinite number of different ways. The symmetry group for N identical particles is therefore the braid group B_N, and anyons emerge as the representations of the group.

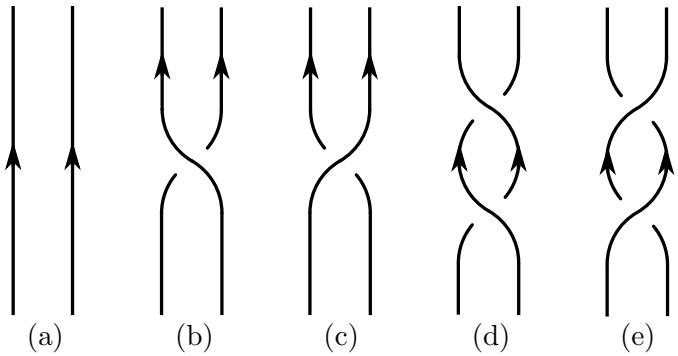

Figure 3.1: Braids and anyons. We consider five kinds of exchanges of identical particles, whose worldlines are shown in (a) $\sim$ (e). In d ≥ 3, (a), (d), (e) and (b), (c) are two kinds of topologically equivalent exchanges. In 2d, all five exchanges, or braids, are different, and the representation of the braid group determines the type of the anyons.

3.2 From a chain to a ladder: non-interacting model

As a first step towards 2d, we couple two chains and consider a ladder model. Again, before plunging into the full interacting model, we first examine a non-interacting one. We note that for a 2d Majorana system there is a consistency condition on the coupling parameters, known as the Grosfeld-Stern rule[10], which requires that the accumulated phase ϕ along a closed loop is related to the number of vertices n by

$$\phi = \frac{\pi}{2}(n-2) \tag{3.1}$$

The sign convention we choose is shown in Fig. 3.2, and the Hamiltonian

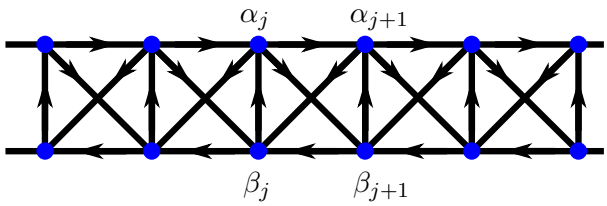

Figure 3.2: Majorana ladder model. The arrows denote the sign of each coupling, in agreement with the Grosfeld-Stern rule.

is

$$\begin{aligned} H = i\sum_j \left(t + m(-1)^j\right)\left(\alpha_j\alpha_{j+1} - \beta_j\beta_{j+1}\right) + it_1\sum_j \beta_j\alpha_j \\ + it_2\sum_j (\alpha_j\beta_{j+1} - \beta_j\alpha_{j+1}) \end{aligned} \tag{3.2}$$

where $t \pm m$ are the intra-chain couplings and $t_{1,2}$ are the inter-chain couplings. Note that $t_{1,2}$ have a different meaning in the previous chapter, and their role is played by m here. We go to the momentum space using Eq. 2.3

$$H = \sum_k \Psi_k^\dagger H_k \Psi_k$$

$$\Psi_k = (\alpha_{k,\text{even}}, \beta_{k,\text{even}}, \alpha_{k,\text{odd}}, \beta_{k,\text{odd}})^T$$

$$H_k = i\begin{pmatrix} 0 & 0 & 0 & 0 \\ t_1 & 0 & 0 & 0 \\ -(t+m)+(t-m)e^{-ik} & t_2(1+e^{-ik}) & 0 & 0 \\ -t_2(1+e^{-ik}) & (t+m)-(t-m)e^{-ik} & t_1 & 0 \end{pmatrix} + h.c. \tag{3.3}$$

In general, diagonalizing a 4×4 hermitian matrix is quite laborious, and useful information is hard to extract. (It is always possible since the problem reduces to a quartic equation, whose root formula is known.) Fortunately, for certain matrices there is a nice trick. A hermitian matrix can always be expanded by $(I, \boldsymbol{\sigma}) \otimes (I, \boldsymbol{\tau})$, where $\boldsymbol{\sigma}$ and $\boldsymbol{\tau}$ are Pauli matrices. If there are not too many terms, upon squaring and rearranging the matrix a few times it will become proportional to unit matrix, with the cross terms cancelled out by the anticommutation relations. In the current situation, we have

$$\begin{aligned} H_k = t_1\sigma^y - t_2(1+\cos k)\,\sigma^y\tau^x + t_2\sin k\,\sigma^y\tau^y \\ + \left((t-m)\cos k - (t+m)\right)\sigma^z\tau^y \\ + (t-m)\sin k\,\sigma^z\tau^x \end{aligned} \tag{3.4}$$

and the spectrum is

$$\begin{aligned} E = \Big(& t_1^2 + t_2^2(1+\cos k)^2 + t_2^2 \sin^2 k + \big((t-m)\cos k - (t+m)\big)^2 \\ & + (t-m)^2 \sin^2 k \pm 2t_2 \Big(t_1^2 \left((1+\cos k)^2 + \sin^2 k\right) \\ & + \big((1+\cos k)\left((t-m)\cos k - (t+m)\right) + \sin^2 k (t-m)\big)^2 \Big)^{\frac{1}{2}} \Big)^{\frac{1}{2}} \end{aligned} \tag{3.5}$$

This result is rather complicated and we discuss the two cases $m = 0$ and $m \neq 0$ separately. We also formulate a low-energy field theory to obtain more insights.

3.2.1 The $m = 0$ case

Now the energy spectrum can be further simplified to

$$E = \sqrt{4t^2 \sin^2 \frac{k}{2} + \left(t_1 \pm 2t_2 \cos \frac{k}{2}\right)^2} \tag{3.6}$$

The system is gapped for general t, t_1 and t_2, but becomes gapless when $t_1 = 2t_2$. To see this, we note that both terms under the square root must be 0 in order that the system is gapless. The first term is 0 only when $\sin \frac{k}{2} = 0$, and thus $t_1 \pm 2t_2 = 0$. The phase diagram is shown in Fig. 3.3.

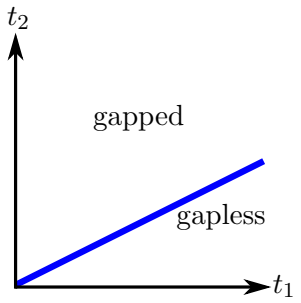

Figure 3.3: Phase diagram of the $m = 0$ Majorana ladder model. The gapless region is the line $t_1 = 2t_2$.

3.2.2 The $m \neq 0$ case

The spectrum is more complicated. To proceed, we restrict out attention to not too large m, so that the spectrum does not change too much. A corollary

is that the E is small only around $k = 0$. We also note that $\frac{\partial E}{\partial k}|_{k=0} = 0$, since only $\cos k$ and $\sin^2 k$ are present in E. Combining this with the fact that $E \geq 0$ and E is smooth, we expect $E = 0$ can only occur at $k = 0$

$$\begin{aligned} E|_{k=0} &= \left(t_1^2 + 4t_2^2 + 4m^2 \pm 4t_2(t_1^2 + 4m^2)^{\frac{1}{2}}\right)^{\frac{1}{2}} \\ &= \left|2t_2 \pm \sqrt{t_1^2 + 4m^2}\right| \end{aligned} \tag{3.7}$$

and the gapless condition follows

$$t_2 = \sqrt{\left(\frac{t_1}{2}\right)^2 + m^2} \tag{3.8}$$

The upshot is that the gapless region is not removed, but shifted. While this does not pose a problem in the ladder model, when we go to 2d things become tricky. The discussion is postponed to Chapter 4.

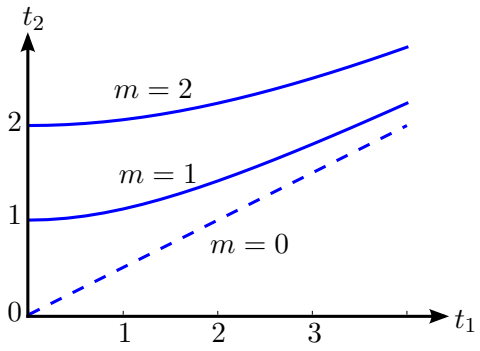

Figure 3.4: Phase diagram of the Majorana ladder model. The gapless region is shifted as one turns on m.

3.2.3 Low-energy field theory

To gain more insight into the relation between the ladder and the chain, we now adopt a low-energy field theoretic view. To do so we assume the

operators on even/odd sites change slowly so that

$$\begin{aligned}
&\sum_j \to \int \mathrm{d}x \\
&\alpha_{2j} \to \alpha_1(x) \\
&\alpha_{2j+2} \to \alpha_1(x) + 2\frac{\partial \alpha_1}{\partial x} \\
&\alpha_{2j-1} \to \alpha_2(x) \\
&\alpha_{2j+1} \to \alpha_2(x) + 2\frac{\partial \alpha_2}{\partial x}
\end{aligned} \tag{3.9}$$

and similar for β's. The low-energy Hamiltonian reads

$$\begin{aligned}
H = 2i \int \mathrm{d}x \left(m\alpha_1\alpha_2 + (t+m)\alpha_1\alpha_2' - (\alpha \leftrightarrow \beta) \right) + it_1 \int \mathrm{d}x \left(\beta_1\alpha_1 + \beta_2\alpha_2 \right) \\
+ it_2 \int \mathrm{d}x \left(\alpha_1\beta_2 + \alpha_2\beta_1 + 2\alpha_1\beta_2' - (\alpha \leftrightarrow \beta) \right)
\end{aligned} \tag{3.10}$$

We further define

$$\begin{aligned}
\alpha_{R/L} &= (\alpha_1 \pm \alpha_2)/2 \\
\beta_{R/L} &= (\beta_1 \mp \beta_2)/2
\end{aligned} \tag{3.11}$$

and in terms of these operators the Hamiltonian finally becomes

$$\begin{aligned}
H = 2i \int \mathrm{d}x \left(2m\alpha_L\alpha_R + (t+m)(\alpha_R\alpha_R' - \alpha_L\alpha_L') + (\alpha \leftrightarrow \beta) \right) \\
+ 2it_1 \int \mathrm{d}x \left(\beta_R\alpha_L + \beta_L\alpha_R \right) \\
+ 4it_2 \int \mathrm{d}x \left(\alpha_R\beta_L - \alpha_L\beta_R - \alpha_R\beta_R' + \alpha_L\beta_L' \right)
\end{aligned} \tag{3.12}$$

where we have ignored the total derivative or boundary terms. In the isolated chain limit, $t_1 = t_2 = 0$, the Hamiltonian reduces to the sum of two chains, of which the physical meaning is clear: within each chain there is a right-moving mode and a left-moving mode, with velocity $\pm 2t$. A nonzero m couples both modes, just like a mass term in the high-energy context, hence the nomenclature. For $m = 0$, the two modes contribute to the low energy states and explains the gaplessness of each chain.

When $m = 0$, a general inter-chain coupling t_1 and t_2 couples all the four modes and thus gap out the spectrum. However, from Eq. 3.12 it is easy

to see that if one chooses $t_1 = 2t_2$, only two out of four modes are coupled, and we are left with two chiral gapless modes on the edge. This analysis is readily generalizable to a 2d model, where a similar coupling scheme will gap out all the bulk modes but leave two edge modes untouched, as we will discuss in detail in Chapter 4.

3.3 From a chain to a ladder: interacting model

Equipped with the insights from the non-interacting model, we now explore the full interacting model, Fig. 3.5, with intra-chain spin-spin and spin-Majorana couplings. The Hamiltonian is

$$\begin{aligned} H = & it\sum_j(\alpha_j\alpha_{j+1} - \beta_j\beta_{j+1}) - igt\sum_j\left(\alpha_j\alpha_{j+1}\mu^z_{j,a} - \beta_j\beta_{j+1}\mu^z_{j,b}\right) \\ & + it_1\sum_j \beta_j\alpha_j + it_2\sum_j(\alpha_j\beta_{j+1} - \beta_j\alpha_{j+1}) \\ & + J\sum_j(\mu^z_{j,a}\mu^z_{j+1,a} + \mu^z_{j,b}\mu^z_{j+1,b}) - h\sum_j(\mu^x_{j,a} + \mu^x_{j,b}) \end{aligned} \tag{3.13}$$

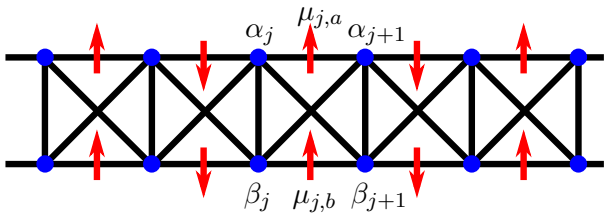

Figure 3.5: Majorana-Ising ladder model. The sign convention is the same as in Fig. 3.2 and we suppress the arrows for clarity.

We expect the success of MFT in the chain model will persist in the

ladder model, with the MFT Hamiltonian

$$\begin{aligned} H_{\text{MFT}} = & it\sum_j(\alpha_j\alpha_{j+1} - \beta_j\beta_{j+1}) \\ & - igt\sum_j\left(\alpha_j\alpha_{j+1}\langle\mu^z_{j,a}\rangle - \beta_j\beta_{j+1}\langle\mu^z_{j,b}\rangle\right) \\ & + it_1\sum_j\beta_j\alpha_j + it_2\sum_j(\alpha_j\beta_{j+1} - \beta_j\alpha_{j+1}) \\ & + J\sum_j(\mu^z_{j,a}\mu^z_{j+1,a} + \mu^z_{j,b}\mu^z_{j+1,b}) - h\sum_j(\mu^x_{j,a} + \mu^x_{j,b}) \end{aligned} \tag{3.14}$$

By the same argument as in the chain model, the limiting cases $h \to 0, \infty$ correspond to $m \neq 0$ and $m = 0$ in the non-interacting model, respectively. If we fix $t_1 = 2t_2$, they further correspond to a gapped phase and an Ising phase. Crucially, there is only one copy of Ising CFT in the latter. Thus, as we tune h from 0 to ∞, we expect a TCI transition in between, where the number of TCI CFT is also one. Furthermore, as the Ising CFT is chiral, so should be the TCI CFT. We illustrate the argument in Fig. 3.6.

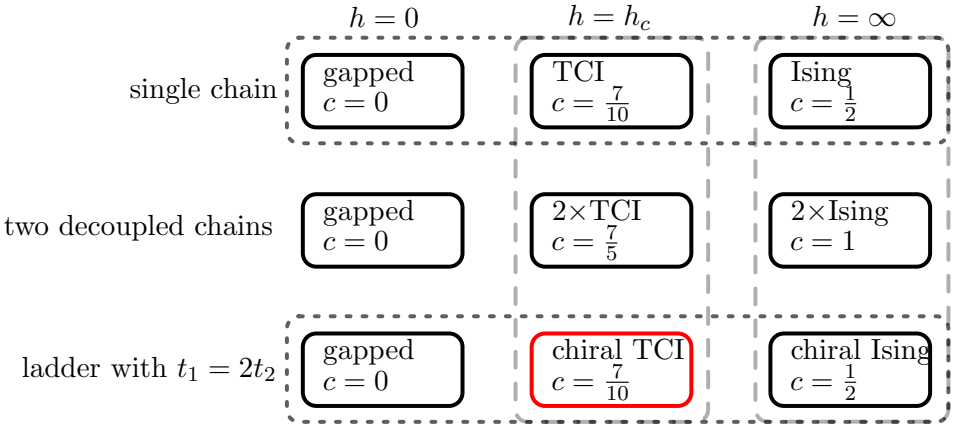

Figure 3.6: From a chain to a ladder. We are interested in the chiral TCI CFT in the red box. A comparison between the first and the third row implies a TCI CFT, while one between the second and the third column suggests that it is chiral. This argument is verified by the DMRG calculations.

3.4 DMRG results

We perform extensive DMRG simulations to confirm the analytical analysis in the previous section. For bookkeeping we copy here the spin-version Hamiltonian

$$\begin{aligned} H = &-t\sum_j(\sigma_j^x\sigma_{j+1}^y + \sigma_j^y\sigma_{j+1}^x) + gt\sum_j\left(\sigma_j^y\sigma_{j+1}^x\mu_{j,a}^z + \sigma_j^x\sigma_{j+1}^y\mu_{j,b}^z\right) \\ &- t_1\sum_j\sigma_j^z + t_2\sum_j(\sigma_j^x\sigma_{j+1}^x + \sigma_j^y\sigma_{j+1}^y) \\ &+ J\sum_j(\mu_{j,a}^z\mu_{j+1,a}^z + \mu_{j,b}^z\mu_{j+1,b}^z) - h\sum_j(\mu_{j,a}^x + \mu_{j,b}^x) \end{aligned} \tag{3.15}$$

where α_j and β_j become σ_j under the Jordan-Wigner transformation, as shown in Fig. 3.7.

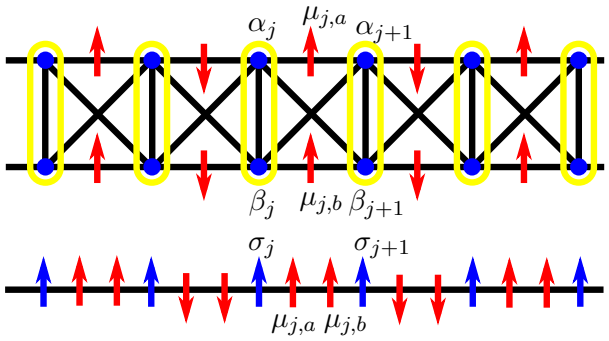

Figure 3.7: The spin model after Jordan-Wigner transformation.

First, we take $t_1 = t_2 = 0$, i.e. the case of two isolated chains. We expect the central charge to be twice of a single chain. The result is shown in Fig. 3.8.

Next, we take $t_1 = 2t_2 = 2$, 1, 0.4. We expect that only one pair of chiral edge modes survive. The result is shown in Fig. 3.9.

We also explore the case $t_1 \neq 2t_2$. We take $t_1 = 1$ and $t_2 = 0.8$. Since the Majorana degrees of freedom are gapped out, we expect the system is dominated by the spin ladder, and an Ising transition lies between two gapped phases. The result is shown in Fig. 3.10.

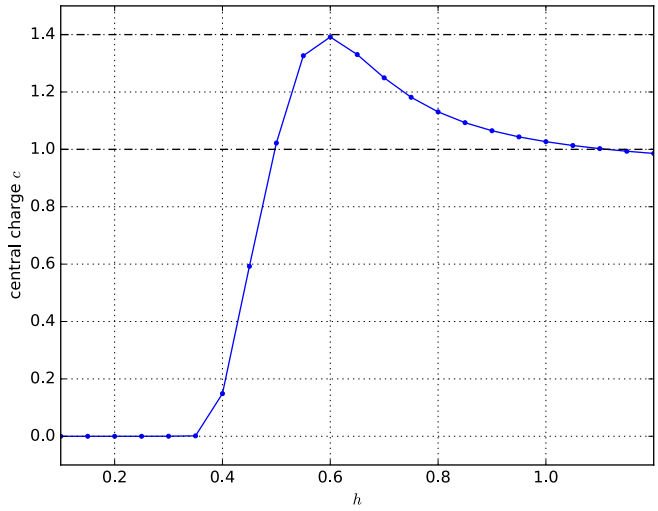

Figure 3.8: Decoupled Majorana-Ising ladder. The central charge is twice that of a chain. We take $L = 24$, $g = 1$, $J = 0.3$ here.

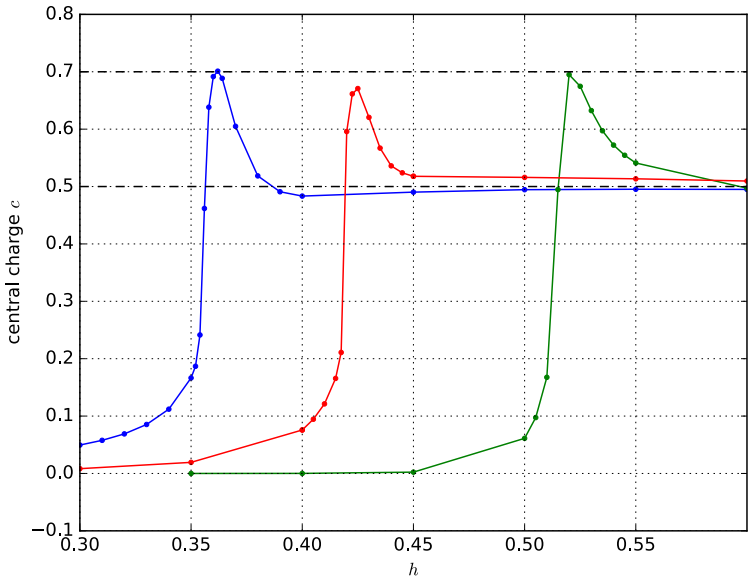

Figure 3.9: Majorana-Ising ladder with $g = 1$, $J = 0.3$, $t_1 = 2t_2 = 2$ (blue), 1 (red), 0.4 (green). All three cases exhibit a TCI transition.

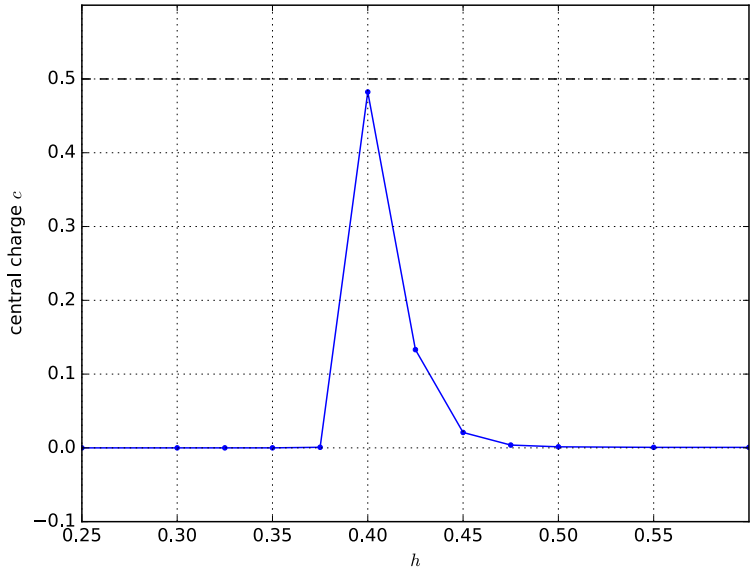

Figure 3.10: Majorana-Ising ladder with $L = 60$, $g = 1$, $J = 0.3$, $t_1 = 1$, $t_2 = 0.8$. There is a Ising transition between two gapped phases.

Chapter 4

From a ladder to 2d

As motivated in Chapter 3, the ultimate goal is to probe a 2d model. Unfortunately, DMRG is impeded by the area law and a direct simulation is out of the question. In this chapter we first analytically discuss the 2d model from various aspects in Section 4.1. Then we introduce a useful concept, known as the entanglement spectrum, and discuss its relevance to the edge gapless modes in Section 4.2. We also discuss the numerical techniques. An application of the approach to the non-interacting model is shown in Section 4.3.

4.1 The 2d model

4.1.1 The non-interacting model

The Hamiltonian of the 2d non-interacting Majorana model is

$$\begin{aligned} H = i\sum_{ij}\left((-1)^i t - m\right)\gamma_{i,j}\gamma_{i+1,j} - it_1\sum_{ij}(-1)^i\gamma_{i,j}\gamma_{i,j+1} \\ + it_2\sum_{ij}(\gamma_{i,j}\gamma_{i-1,j+1} - \gamma_{i,j}\gamma_{i+1,j+1}) \end{aligned} \tag{4.1}$$

The advantage of studying a ladder model is that we have direct access to the edge states in the analytical solution, which is unfortunately not the case for a 2d model. Here, we can only solve the bulk spectrum. As usual

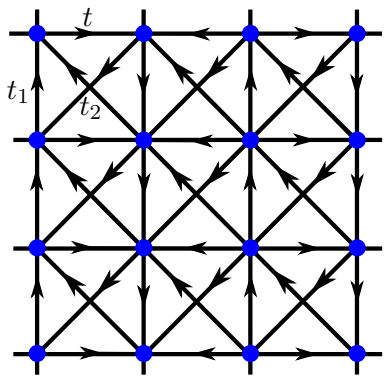

Figure 4.1: The 2d non-interacting model. Note that we have use a different convention than in the previous chapter to have a minimun unit cell.

we go to the momentum space

$$\begin{aligned}
\alpha_{k_x,k_y} &= \sqrt{\frac{1}{2N}} \sum_{ij} e^{ik_x 2i + ik_y j} \gamma_{2i,j} \\
\beta_{k_x,k_y} &= \sqrt{\frac{1}{2N}} \sum_{ij} e^{ik_x (2i+1) + ik_y j} \gamma_{2i+1,j} \\
\gamma_{2i,j} &= \sqrt{\frac{2}{N}} \sum_{k_x k_y} e^{-ik_x 2i - ik_y j} \alpha_{k_x,k_y} \\
\gamma_{2i+1,j} &= \sqrt{\frac{2}{N}} \sum_{k_x k_y} e^{-ik_x (2i+1) - ik_y j} \beta_{k_x,k_y}
\end{aligned} \tag{4.2}$$

In momentum space the Hamiltonian reads

$$\begin{aligned}
H &= \sum_{\boldsymbol{k}} \Psi^\dagger_{\boldsymbol{k}} H_{\boldsymbol{k}} \Psi_{\boldsymbol{k}} \\
\Psi_{\boldsymbol{k}} &= (\alpha_{\boldsymbol{k}}, \beta_{\boldsymbol{k}})^T
\end{aligned} \tag{4.3}$$

with

$$\begin{aligned}
H_{\boldsymbol{k}} &= 2 \begin{pmatrix} -t_1 \sin k_y & it \cos k_x - (m + 2t_2 \cos k_y) \sin k_x \\ -it \cos k_x - (m + 2t_2 \cos k_y) \sin k_x & t_1 \sin k_y \end{pmatrix} \\
&= -2 \sin k_x (m + 2t_2 \cos k_y) \sigma^x - 2t \cos k_x \sigma^y - 2t_1 \sin k_y \sigma^z
\end{aligned} \tag{4.4}$$

and we immediately get the bulk spectrum

$$E = 2\sqrt{\sin^2 k_x (m + 2t_2 \cos k_y)^2 + t^2 \cos^2 k_x + t_1^2 \sin^2 k_y} \tag{4.5}$$

It is straightforward to see when the bulk spectrum is gapless. The three terms are all zero only when

$$\begin{aligned} &\cos k_x = \sin k_y = m + 2t_2 \cos k_y = 0 \\ \Rightarrow k_x = \pm\frac{\pi}{2},\ &\begin{cases} m = 2t_2 \\ k_y = \pi \end{cases} \text{ or } \begin{cases} m = -2t_2 \\ k_y = 0 \end{cases} \end{aligned} \tag{4.6}$$

We can calculate the Chern number of the system from the low energy points in the Brillouin zone[11], where the Hamiltonian is

$$\begin{aligned} H_{(-\frac{\pi}{2},0)} &= 2(m + 2t_2)\sigma^x - 2tq_x\sigma^y - 2t_1 q_y \sigma^z \\ H_{(-\frac{\pi}{2},\pi)} &= 2(m - 2t_2)\sigma^x - 2tq_x\sigma^y + 2t_1 q_y \sigma^z \\ H_{(\frac{\pi}{2},0)} &= -2(m + 2t_2)\sigma^x + 2tq_x\sigma^y - 2t_1 q_y \sigma^z \\ H_{(\frac{\pi}{2},\pi)} &= -2(m - 2t_2)\sigma^x + 2tq_x\sigma^y + 2t_1 q_y \sigma^z \end{aligned} \tag{4.7}$$

and the Chern number follows

$$n = \frac{1}{2}\sum \text{sign}(v_x v_y \Delta) = \begin{cases} 0 & \text{if } |m| > 2t_2 \\ 2 & \text{if } |m| < 2t_2 \end{cases} \tag{4.8}$$

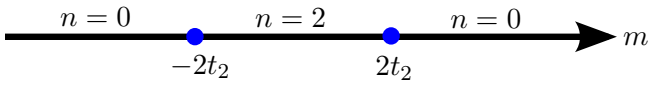

Figure 4.2: The phase diagram of the 2d non-interacting model. A non-zero Chern number n signifies a topological phase and a chiral edge mode. Note that since we "double" the Hilbert space in a Majorana system, the Chern number we get is twice the real value. Also, the values of t and t_1 are irrelevent as long as they remain positive.

The upshot of this calculation is that, the edge of the 2d system is similar to the ladder case, with a gapless phase and a gapped phase, which is determined by m. However, there are two noteworthy differences between the 2d and the ladder case. In the latter, an infinitesimal m will gap out the spectrum, while in the former the transition happens at $m = 2t_2$, a finite

value. Moreover, in 2d the bulk spectrum becomes gapless at the transition point, a fact obscured in the ladder case, as there is not a well-defined "bulk" for a ladder.

The edge mode is best understood from the low-energy theory. We recall that when $m = 0$ there is a left-moving mode and a right-moving mode within each chain, and the t_1 and t_2 terms gap out these modes except when $t_1 = 2t_2$, in which case only a pair of modes are gapped out and another pair is left untouched. As we introduce more chains, the new t_1 and t_2 terms will successively gap out the bulk modes, and leave a pair of edge modes gapless. As the edge modes become macroscopically separated, we can relax the constrain of $t_1 = 2t_2$ and the gapless modes will persist, as seen from the Chern number calculation.

We now convert the analysis into equations. We perform the substitution

$$\begin{aligned} \sum_i &\to \frac{1}{2}\int \mathrm{d}x \\ \gamma_{2i,j} &\to (-1)^i \alpha_j^1 \\ \gamma_{2i+1,j} &\to (-1)^i \alpha_j^2 \end{aligned} \tag{4.9}$$

and define

$$\alpha_j^{R/L} = (\alpha_j^1 \pm \alpha_j^2)/2 \tag{4.10}$$

Then the Hamiltonian becomes

$$\begin{aligned} H \to{}& 2i\sum_j \int \mathrm{d}x \left(-m\alpha_j^1\alpha_j^2 + (t+m)\alpha_j^2\alpha_j^{1'}\right) \\ & - it_1 \sum_j \int \mathrm{d}x \, (\alpha_j^1\alpha_{j+1}^1 - \alpha_j^2\alpha_{j+1}^2) \\ & + 2it_2 \sum_j \int \mathrm{d}x \big(-\alpha_j^1\alpha_{j+1}^2 + \alpha_j^2\alpha_{j+1}^1 + \alpha_j^1\alpha_{j+1}^{2'} + \alpha_j^2\alpha_{j+1}^{1'}\big) \\ ={}& 2i\sum_j \int \mathrm{d}x \left(2m\alpha_j^R\alpha_j^L + (t+m)(\alpha_j^R\alpha_j^{R'} - \alpha_j^L\alpha_j^{L'})\right) \\ & - 2it_1 \sum_j \int \mathrm{d}x \, (\alpha_j^R\alpha_{j+1}^L + \alpha_j^L\alpha_{j+1}^R) \\ & + 4it_2 \sum_j \int \mathrm{d}x \, (\alpha_j^R\alpha_{j+1}^L - \alpha_j^L\alpha_{j+1}^R + \alpha_j^R\alpha_{j+1}^{R'} - \alpha_j^L\alpha_{j+1}^{L'}) \end{aligned} \tag{4.11}$$

When $m = 0$ and $t_1 = 2t_2$, the $\alpha_j^R\alpha_{j+1}^L$ terms vanish while the $\alpha_j^L\alpha_{j+1}^R$ terms

gap out all the gapless modes except α_1^R and α_N^L. Thus this pair of edge modes remains gapless.

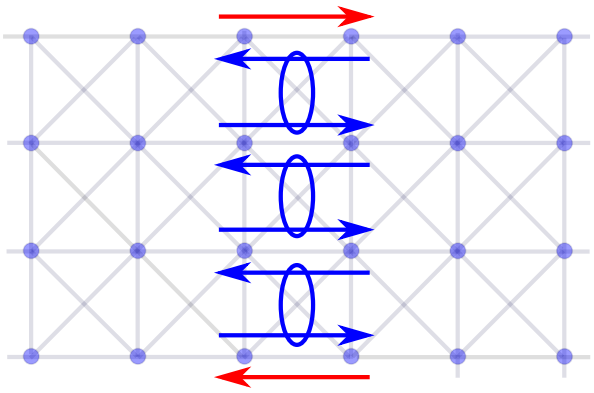

Figure 4.3: The edge modes from the low-energy theory. While the bulk modes are gapped out, the edge modes are left gapless.

4.1.2 The interacting model

The Hamiltonian of interacting model is

$$\begin{aligned} H = & it\sum_{ij}(-1)^i\left(1-g\mu_{ij}^z\right)\gamma_{i,j}\gamma_{i+1,j} - it_1\sum_{ij}(-1)^i\gamma_{i,j}\gamma_{i,j+1} \\ & + it_2\sum_{ij}(\gamma_{i,j}\gamma_{i-1,j+1} - \gamma_{i,j}\gamma_{i+1,j+1}) \\ & + J\sum_{ij}\mu_{ij}^z\mu_{i,j+1}^z - h\sum_{ij}\mu_{ij}^x \end{aligned} \tag{4.12}$$

and the corresponding MFT one is, as before,

$$\begin{aligned} H = & it\sum_{ij}(-1)^i\left(1-g\langle\mu_{ij}^z\rangle\right)\gamma_{i,j}\gamma_{i+1,j} - it_1\sum_{ij}(-1)^i\gamma_{i,j}\gamma_{i,j+1} \\ & + it_2\sum_{ij}(\gamma_{i,j}\gamma_{i-1,j+1} - \gamma_{i,j}\gamma_{i+1,j+1}) \\ & + J\sum_{ij}\mu_{ij}^z\mu_{i,j+1}^z - h\sum_{ij}\mu_{ij}^x \end{aligned} \tag{4.13}$$

At $h = \infty$, we again obtain a non-interacting, $m = 0$ Majorana model. We expect the edge modes to be an Ising CFT, a story we are familiar up to

now. As $h \to 0$, however, there are two possible scenarios. If g is not large enough and thus m is not large enough either, the system will stay in the original phase. For a large g, a large m will gap out the edge modes. Thus, we can still expect a TCI point in between the two limits of h.

Based on the ladder model calculation, we can also formulate a "coupled-chain" analysis. As we couple two TCI chains with appropriate coupling parameters, we have seen that a pair of right and left movers are gapped out and the other pair left untouched. If we further introduce more TCI chains, we expect the bulk movers will be consecutively gapped out with the edge modes gapless. As we have seen from the previous section, this analysis works well for the non-interacting model with Ising CFT.

To sum up, we expect a TCI edge mode to occur as we tune the h from 0 to ∞, while, on the other hand, the bulk is gapped, as hinted from the MFT and the coupled-chain analysis. There is another possibility that is not so interesting, though. As $h = 0$ and $h = \infty$ correspond to topologically different phases, there might be just a "common" phase transition in between, where the bulk is gapless and edge modes are ill defined. Due to lack of numerical probes, we can not assert which one is correct at this point.

4.2 Entanglement spectrum, edge modes and infinite DMRG

In order to numerically explore the nature of the edge modes, new techniques are necessary. For our present purpose, a measurement of the entanglement spectrum with infinite DMRG seems to be most promising.

Back in Section 2.4, we defined the entanglement entropy from a bipartition of a system

$$S_A = \mathrm{Tr}(\rho_A \ln \rho_A) \tag{4.14}$$

Apparently, much information stored in ρ_A is lost in this quantity, and this motivates the definition of the entanglement spectrum, first proposed by Li and Haldane[12]

$$E_\alpha = -\log \rho_{A,\alpha} \tag{4.15}$$

where $\rho_{A,\alpha}$'s are the eigenvalues of ρ_A. People then realize that, generally, the entanglement spectrum resembles the edge states spectrum of a topological phase, up to a shift and rescaling [13].

The infinite DMRG algorithm turns out to be a powerful method of extracting the entanglement spectrum[14]. Instead of the truly 2d model that is beyond the capacity of DMRG, one considers a cylinder geometry,

with $L_x \lesssim 10$ and $L_y = \infty$. By choosing an appropriate DMRG path, the entanglement spectrum is easily obtained from the MPS. We will elaborate this idea in the next section using a concrete example.

4.3 The non-interacting model revisited

We go back to the non-interacting model with a cylinder geometry and measure the entanglement spectrum. We consider the $\infty \times 4$ and $\infty \times 8$ cases. Upon a Jordan-Wigner transformation, the spin models have sizes of $\infty \times 2$ and $\infty \times 4$, respectively. The DMRG paths are shown in Fig. 4.4.

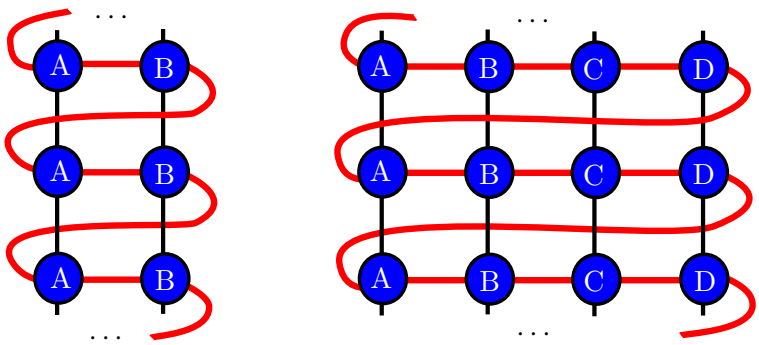

(a) (b)

Figure 4.4: The DMRG paths for the non-interacting model with a cylinder geometry, with the size of (a) $\infty \times 4$ and (b) $\infty \times 8$ in the Majorana basis, or (a) $\infty \times 2$ and (b) $\infty \times 4$ in the spin basis.

For the $\infty \times 4$ case, the entanglement spectrum is readily identified with the Ising CFT result, see Fig. 4.5. The spectrum follows a pattern of "1101111122223". The $\infty \times 8$ case is more complicated. Now there is more than one copy of Ising CFT on the edge, and we need to calculate the transverse lattice momentum to tell them apart and identify the pattern. To do so we follow the methods in [14] and find the (diagonal) fixed point of the "twisted transfer matrix" (TTM), whose diagonal elements are the corresponding spacial translation phases e^{ika}, where the momentum k can be extracted. The construction of the TTM is shown diagrammatically in Fig. 4.6 We shift the k's by a multiple of 2π so that the pattern is clearly visible. The result is shown in Fig. 4.7.

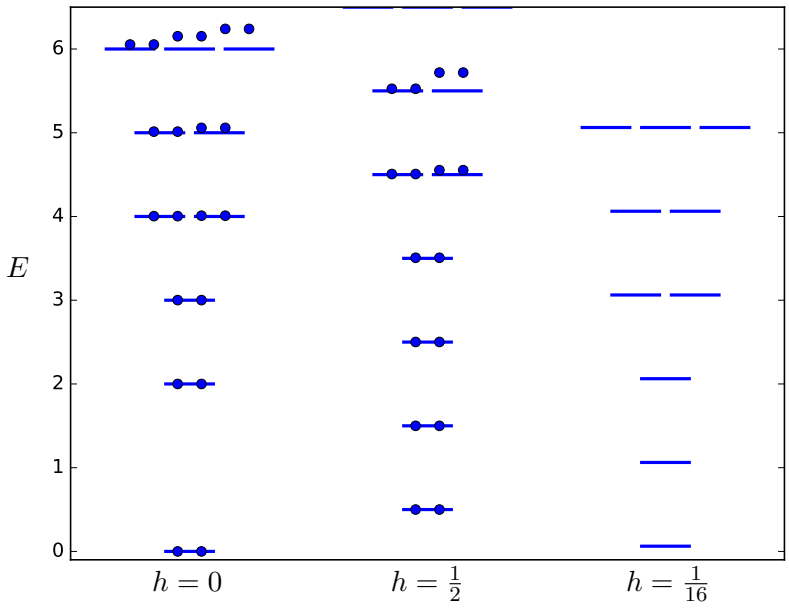

Figure 4.5: The CFT towers and the entanglement spectrum. The lines are given by the Ising CFT which contains three conformal towers. The dots are the entanglement spectrum from infinite DMRG upon a shift and rescaling. We see an almost perfect match here.

Finally, we briefly discuss the difficulties of applying this technique to the interacting model. As can be already seen from the $\infty \times 8$ case, the conformal towers are mixed together, and resolving each tower becomes even harder for a TCI CFT where there are five possible towers. In [14] and other works adopting this method, there exists an additive conserved quantum number, e.g. total spin in z direction S_z or total particle number n, that helps to distinguish between different towers, a feature we unfortunately lack in our model. This drawback might be compensated for by more sophisticated considerations of CFT, a direction worth exploring.

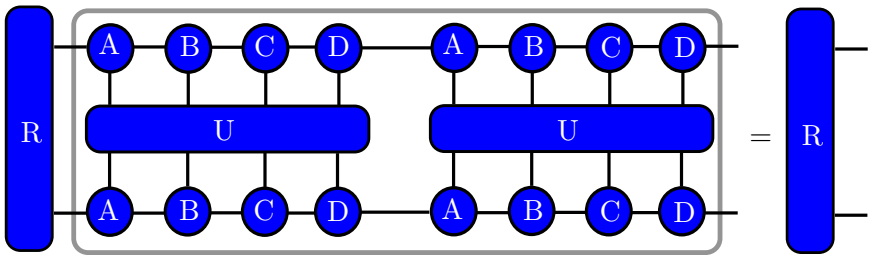

Figure 4.6: The twisted transfer matrix (TTM) and the transverse momentum. The twisted transfer matrix is constructed by multiplicating the MPS with a unitry transformation U which rotates the cylinder by a lattice constant. The fixed point R is diagonal and the diagonal elements are e^{ika}.

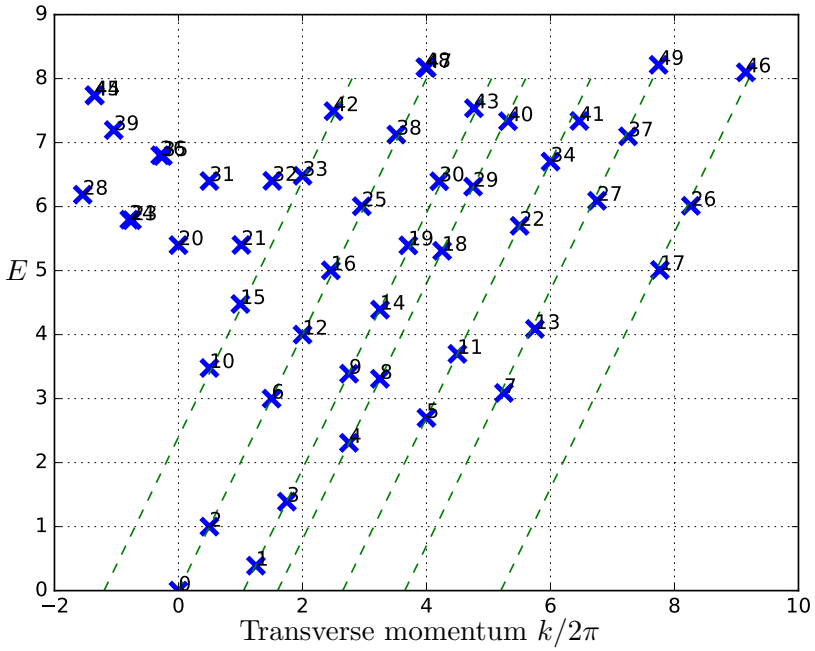

Figure 4.7: The entanglement spectrum of the $\infty \times 8$ case. Here to tell apart different conformal towers the transverse momentum is measured and translated by a multiple of 2π for clarity. We can see that the pattern "110111112" holds for every tower.

Chapter 5

Conclusion

In this thesis, the main result is the generalization of the GSV model to a ladder model and the identification of the TCI edge mode.

In the GSV model, a TCI transition is obtained by tuning only one parameter. By examining the chain model, we establish a mean field theory that agrees with the limiting cases of the full interacting model, which hints a TCI transition as we tune the parameter. The mean field theory is readily generalized to a ladder and further to 2d.

Based on the results from the interacting chain model and the MFT ladder/2d model, we expect a TCI edge mode in the interacting ladder/2d model. We carry out extensive DMRG calculation of the interacting ladder model and the results agree with the analytical argument. To the best of our knowledge, this is the first work where a TCI edge mode is identified.

The DMRG calculations are not applicable in 2d models. Thus so far we can not assert whether the analysis in the interacting ladder model still holds in the interacting 2d model. We discuss a possible numerical probe of the latter using infinite DMRG which has access to the entanglement spectrum, which might give some interesting results in future research.

Bibliography

[1] Tarun Grover, DN Sheng, and Ashvin Vishwanath. Emergent space-time supersymmetry at the boundary of a topological phase. *Science*, 344(6181):280–283, 2014.

[2] Philippe Francesco, Pierre Mathieu, and David Sénéchal. *Conformal field theory*. Springer Science & Business Media, 2012.

[3] Paul Ginsparg. Applied conformal field theory. *arXiv preprint hep-th/9108028*, 1988.

[4] Malte Henkel. *Conformal invariance and critical phenomena*. Springer Science & Business Media, 2013.

[5] Ulrich Schollwöck. The density-matrix renormalization group in the age of matrix product states. *Annals of Physics*, 326(1):96–192, 2011.

[6] `www.itensor.org`.

[7] Pasquale Calabrese and John Cardy. Entanglement entropy and quantum field theory. *Journal of Statistical Mechanics: Theory and Experiment*, 2004(06):P06002, 2004.

[8] Alan J Heeger, S Kivelson, JR Schrieffer, and W-P Su. Solitons in conducting polymers. *Reviews of Modern Physics*, 60(3):781, 1988.

[9] DJ Thouless, Mahito Kohmoto, MP Nightingale, and M Den Nijs. Quantized hall conductance in a two-dimensional periodic potential. *Physical Review Letters*, 49(6):405, 1982.

[10] Eytan Grosfeld and Ady Stern. Electronic transport in an array of quasiparticles in the $\nu = 5/2$ non-abelian quantum hall state. *Physical Review B*, 73(20):201303, 2006.

[11] B Andrei Bernevig and Taylor L Hughes. *Topological insulators and topological superconductors*. Princeton University Press, 2013.

[12] Hui Li and F Duncan M Haldane. Entanglement spectrum as a generalization of entanglement entropy: Identification of topological order in non-abelian fractional quantum hall effect states. *Physical review letters*, 101(1):010504, 2008.

[13] Xiao-Liang Qi, Hosho Katsura, and Andreas WW Ludwig. General relationship between the entanglement spectrum and the edge state spectrum of topological quantum states. *Physical review letters*, 108(19):196402, 2012.

[14] Lukasz Cincio and Guifré Vidal. Characterizing topological order by studying the ground states on an infinite cylinder. *Physical review letters*, 110(6):067208, 2013.

[15] Ettore Majorana. Teoria simmetrica dellelettrone e del positrone. *Il Nuovo Cimento (1924-1942)*, 14(4):171, 1937.

[16] Mark Srednicki. *Quantum field theory*. Cambridge University Press, 2007.

[17] Steven R Elliott and Marcel Franz. Colloquium: Majorana fermions in nuclear, particle, and solid-state physics. *Reviews of Modern Physics*, 87(1):137, 2015.

[18] Jason Alicea, Yuval Oreg, Gil Refael, Felix Von Oppen, and Matthew PA Fisher. Non-abelian statistics and topological quantum information processing in 1d wire networks. *Nature Physics*, 7(5):412–417, 2011.

[19] Chetan Nayak, Steven H Simon, Ady Stern, Michael Freedman, and Sankar Das Sarma. Non-abelian anyons and topological quantum computation. *Reviews of Modern Physics*, 80(3):1083, 2008.

[20] A Yu Kitaev. Unpaired majorana fermions in quantum wires. *Physics-Uspekhi*, 44(10S):131, 2001.

Appendix A

Majorana fermions

Majorana fermions were first proposed by E. Majorana in 1937[15]. He realized, as stated here in a modern way[16][17], that it is possible to define a charge conjugation symmetric solution of the Dirac equation in the sense that

$$\mathcal{C}^{-1}\Psi\mathcal{C} = \Psi \tag{A.1}$$

where $\mathcal{C}$ denotes the charge conjugation operator and Ψ is the second-quantized field operator. By choosing a representation known as Majorana representation where the charge conjugation matrix $C = 1$ and thus $\mathcal{C}^{-1}\Psi\mathcal{C} = C\Psi^* = \Psi^*$, the condition translates to

$$\Psi^{a\dagger} = \Psi^a \tag{A.2}$$

and Ψ^a's, with the fermionic condition $\{\Psi_i^a, \Psi_j^b\} = 2\delta^{ab}\delta_{ij}$ satisfied, are known as Majorana fermion operators. From now on we will use the letter $\gamma^{(a)}$ instead to denote Majorana fermions to emphasize the difference between Majorana and Dirac. Indeed, while the equation of motion is the same, i.e. the Dirac equation, the Lagrangians are different. The relation between the two is analogous to the real and complex scalar fields in the bosonic case[16]. In nonrelativistic systems, we are free from the spin-statistics theorem, and it is legitimate to regard γ's as spinless Majorana operators with no spin indices. Below we will mainly focus on spinless operators.

A few comments are in order. We first note that the Majorana operators can be related to Dirac fermion operators by defining pairwise

$$\gamma_1 = c^\dagger + c,\ \gamma_2 = i(c^\dagger - c) \tag{A.3}$$

Using this transformation, we can always map a fermionic Hamiltonian into a Majorana one, and vice versa. Thus, paired Majorana fermions are abundant in electronic systems, giving an equivalent, though not interesting, representation. What we are interested in, as a result, are only the unpaired ones. Another scenario where Majorana fermions appear "trivially" is in ordinary superconductors. In the BdG mean field approach, Cooper pairing are accounted for by a bilinear pairing term $\Delta c^\dagger c^\dagger + h.c.$ A sage and almost

unique choice of field operator for Hamiltonians of this kind is the Nambu spinor, defined as $\Psi = \left(c_\uparrow, c_\downarrow, c_\downarrow^\dagger, -c_\uparrow^\dagger\right)^T$. The fact that excitations in this system are Majorana fermions follows from $C\Psi^* = \Psi$, where $C = \tau^y\sigma^y$ and $\boldsymbol{\sigma}$ and $\boldsymbol{\tau}$ are Pauli matrices in spin and Nambu spaces, respectively. While this is conceptually interesting, the Majorana excitations are not local and further manipulations are hindered.

Recently people realize[17] that, unlike the two cases discussed above, zero-energy Majorana excitations typically bound with edges or defects in topological phases, or Majorana zero modes (MZM), have a few nice properties. Apart from being localized in space, they also behave as non-Abelian anyons[18] when braided against each other, allowing potential applications in topological quantum computation[19]. An prototypical realization of MZM is the Kitaev chain model[20]. The Hamiltonian is

$$H = \sum_j \left(-tc_j^\dagger c_{j+1} + \Delta c_j^\dagger c_{j+1}^\dagger + h.c. - \mu c_j^\dagger c_j\right) \tag{A.4}$$

The $\Delta = 0$ case is the familiar tight binding model, and with an appropriate μ it is a topologically trivial insulator. This can be seen from the fact that the phase is connected to the isolated atom limit without closing the gap by continuously decreasing t to 0. Interesting physics appears if we take $\Delta = t$ and $\mu = 0$. In this case, we have

$$H = it\sum_{j=1}^{N-1} \gamma_{j,2}\gamma_{j+1,1} \tag{A.5}$$

where we have used Eq. A.3 for each site to rewrite the Hamiltonian using Majorana operators. Now the bulk Hamiltonian is in a gapped phase, as can be seen by recombining $\gamma_{j,2}$ and $\gamma_{j+1,1}$ into Dirac operators. What is crucial, however, is that $\gamma_{1,1}$ and $\gamma_{N,2}$ do not enter the Hamiltonian, and thus represent two MZMs. Combining these two operators into $f = (\gamma_{1,1} + i\gamma_{N,2})/2$, we can further identify the degenerate ground states $|0\rangle$ and $|1\rangle$ by $f|0\rangle = 0$ and $|1\rangle = f^\dagger|0\rangle$. Since there is only one zero energy state, it is robust against perturbation as long as the particle-hole symmetry is preserved. Note that the Majorana operators are localized at the two edges of the chain. While immune from decoherence induced by local perturbation, the MZMs can be braided by, e.g., introducing a T-junction, allowing potential quantum computational operations.

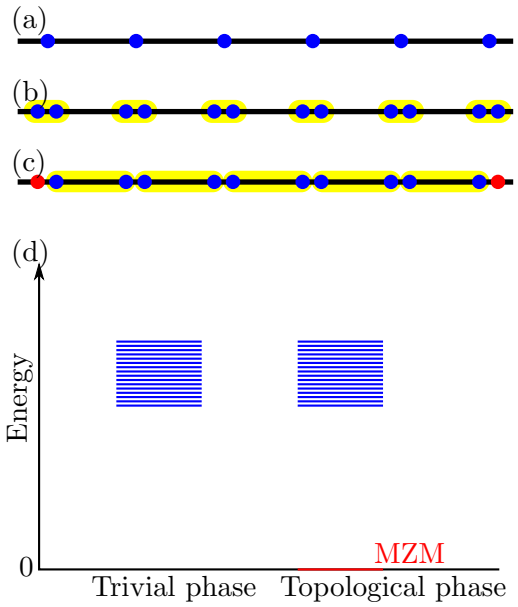

Figure A.1: The Kitaev chain model can be written in Dirac fermion operators (a) or Majorana fermion operators (b)(c). (b) The trivial phase can be continuously connected to the isolated atom limit without closing the gap. (c)(d) In the topological phase, there is a topologically protected zero energy state.